BNL-102249-2014-TECH
RHIC/AP/143;BNL-102249-2013-IR

A Study of Betatron and Momentum Collimators in RHIC

D. Trbojevic

September 1997

Collider Accelerator Department
Brookhaven National Laboratory

U.S. Department of Energy
USDOE Office of Science (SC)

DISCLAIMER

A Study of Betatron and Momentum Collimators in RHIC *

D. Trbojevic, A.J. Stevens, and M. Harrison
Brookhaven National Laboratory, Upton, NY, 11973, USA

Abstract

Two separate accelerator rings in the Relativistic Heavy Ion Collider (RHIC) will provide collisions between equal and unequal heavy ion species up to the gold ions, including the two polarized proton beams. There are six interaction points with two regions with β^*=1-2 m occupied by the large detectors PHENIX and STAR. The transverse and longitudinal emittances of the gold ions are expected to double in size between one to two hours due to intra-beam scattering which may lead to transverse beam loss. Primary betatron collimators are positioned in the ring where the betatron functions have large values to allow efficient removal of particles with large betatron amplitudes. In this report we investigated distributions and losses coming from the out-scattered particles from the primary collimators, as well as the best positions for the secondary momentum and betatron collimators. Additional studies of the detector background due to beam halo and other details about the collimation in RHIC are reported elsewhere (ref. [1] and [2]), while more information about the momentum collimation was previously reported in ref. [10].

1 INTRODUCTION

Collisions of equal or different heavy-ions occur at six interaction regions (IR). Two IR are designed to be at a lower β^*=1-2 m to provide luminosity of the order of $\mathcal{L}$=$10^{27} cm^{-2} s^{-1}$ for gold on gold collisions. Two large detectors, STAR and PHENIX, are located at the high luminosity regions. The strong focusing triplet quadrupoles at opposite sides of interaction points (IP) are the limiting apertures due to the large betatron amplitude functions of the order of $\beta \sim 1500$ m.

Table 1: MAJOR RHIC PARAMETERS

Kinetic energy, Au	10.8 - 100 GeV/u
Kinetic energy, p	28.3 - 250 GeV/u
Number of Bunches	60
Circumference	3833.845 m
Number of IP	6
Betatron Tunes	28.19/29.18
γ_t	22.89
Max Dipole Field	3.45 T
Max quad gradient	71.2 T/m
Arc magnet coil ID	80 mm
Triplet coil ID	130 mm

* Work performed under the auspices of the U.S. Department of Energy

The major RHIC parameters are presented in table 1. The six dimensional emittance of the heavy ion beams is expected to double in size due to intra-beam scattering between one to two hours. Particle amplitudes can also grow due to other effects like beam gas interaction, beam diffusion due to the nonlinear beam dynamics etc. The amplitude growth could result in a beam loss at limiting apertures, like the triplet magnets close to the large detectors, which results in a significant background. A limiting aperture of the collimator can reduce the background. The primary betatron collimator has to be able to remove particles with large amplitudes. As reported earlier [1] the background flux ϕ in a detector can be written as:

$$\phi = N \cdot (1-\epsilon) \cdot P \cdot F, \quad (\text{hits cm}^{-2}\text{s}^{-1}) \qquad (1)$$

where N is the number of particles per unit time on the collimator, (1-ϵ) is the collimator inefficiency, P is the fraction of the outscattered ions interacting in the "local" triplet magnets upstream of the detector, while F is the secondary particle fluence per locally interacting particle. This report studied the distribution of scattered particles from the primary collimators and their propagation throughout the RHIC accelerators - an estimation of the factor P in the above equation. More information about evaluations of the collimator efficiency (*factor* (1-ϵ)) and the hadron cascade calculation factors (*factor F*) is reported in [1]. The first part of the report (section 3) is about the initial conditions: particle's distributions at the primary collimators which are input for the tracking studies. In the second part (section 4), particle distributions of the survived outscattered particles around the rings in both transverse and longitudinal phase spaces are shown. In the next part of the report (sections 6 and 7) distributions of the lost particles around the ring are shown. The optimum location for the secondary betatron and momentum collimator are reported.

2 PRIMARY COLLIMATORS

Positions of the primary collimators in the two RHIC (*blue* and *yellow*) rings are set downstream of the large PHENIX detector at locations with high β value. The efficiency of the betatron collimator improves with higher values of the betatron amplitude function. The best possible locations in the RHIC lattice are about 5-6 m downstream of the high focusing quadrupoles where $\beta \sim$1100 m. An illustration of halo particles encountering a limited aperture of the primary collimator is shown in Fig. 1. The heavy ion beams in RHIC, as gold $^{+79}Au^{197}$, are expected to have a very fast emittance growth due to intra-beam-scattering (IBS) ($\sigma \simeq Z^4/\mathrm{A}^2$). Particles in the bunch exchange longitu-

dinal and transverse momenta by Coulomb scattering. A transverse halo may be created by particles escaped from the *rf* bucket. The initial bunch area grows for almost one

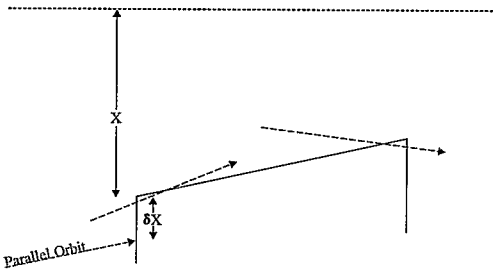

Figure 1: Illustration of halo particles encountering a limiting aperture collimator. Optimal collimation is achieved for orbits parallel to the face of the collimator.

order of magnitude due to the IBS and the transverse emittance is expected to grow from the initial value at injection of ϵ=10 π mm mrad after few hours of store up to ϵ=40 π mm mrad. The halo growth in this study, as we already

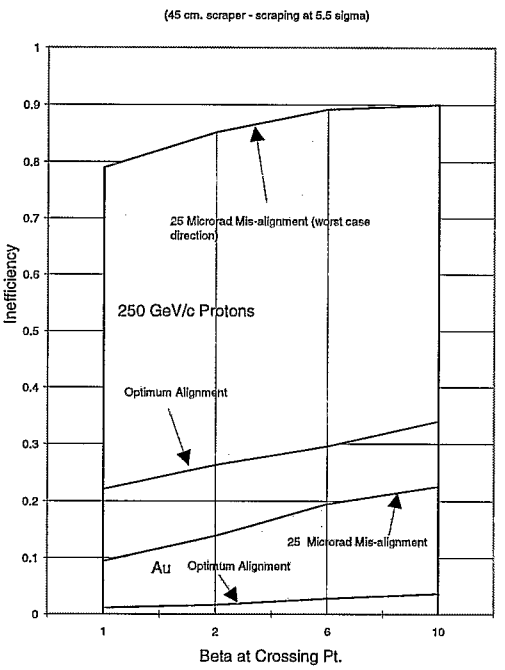

Figure 2: Results for a single pass scraping Inefficiencies

reported [1] is simplified by a diffusion process which was based on measurements in the SPS [6] and [7]. The amplitude growth A is presented [1] as:

$$\delta A = 2.45 \cdot \sigma \cdot e^{(\frac{A}{\sigma}-4)}, \qquad (2)$$

where $\sigma = \sqrt{\epsilon/6\pi\,\beta\gamma}$, the normalized emittance is labeled as ϵ, and $\gamma\beta$ are the relativistic factors. The dynamical aperture of RHIC in the gold ion store was previously [3] estimated to be at the beginning of the store 8 σ while at the end of the 10 hours store 5 σ. The amplitude growth presented above assumed [1] the dynamical aperture of 4σ. The upstream edge of the collimator is set at 5.5 σ with a slope which corresponds to the betatron function slope. Particles which reach the front edge of the collimator are transported through the 0.45 m long collimator by a computer code *ELSHIM* written by Van Ginneken [4]- [5]. The collimator material is assumed to be nickel-copper compound. The emittance of the heavy-ions (gold) is assumed to be 40 π mm mrad, and 20 π mm mrad for the proton beam. A single pass scraping inefficiency as a function of alignment for the gold ions and protons is shown in Fig. 2.

3 INITIAL CONDITIONS

The initial particle distributions are created by particle's orbits which emerge from the collimator without having inelastically interacted with the collimator. Fig. 3 represents

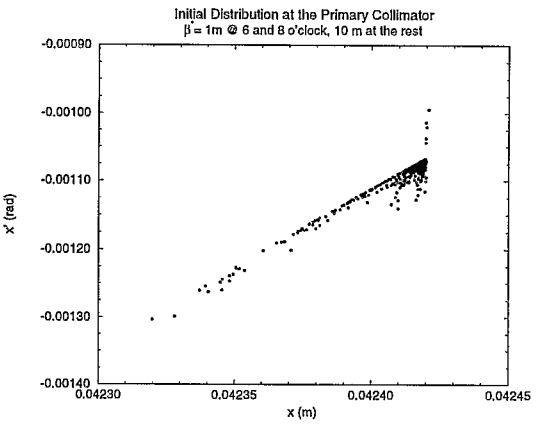

Figure 3: Initial distribution in x-x' phase space of gold ions outscattered from the primary collimator

the initial distribution of outscattered gold ions in the horizontal phase space at the primary collimator. The angle of the scattered ions is very narrow.

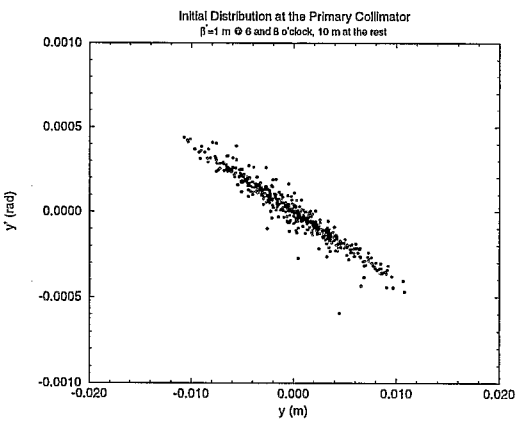

Figure 4: Initial distribution in y-y' phase space of gold ions outscattered from the primary collimator.

Fig. 4 represents the initial outscattered particle distribution in the vertical phase space at the primary collimator. The momentum distribution of the scattered particles from the collimator shows (see Fig. 5) that a large number of particles have momentum offsets much larger than the projected RHIC bucket size at storage $\sigma_p \pm 0.2\%$. A distribution

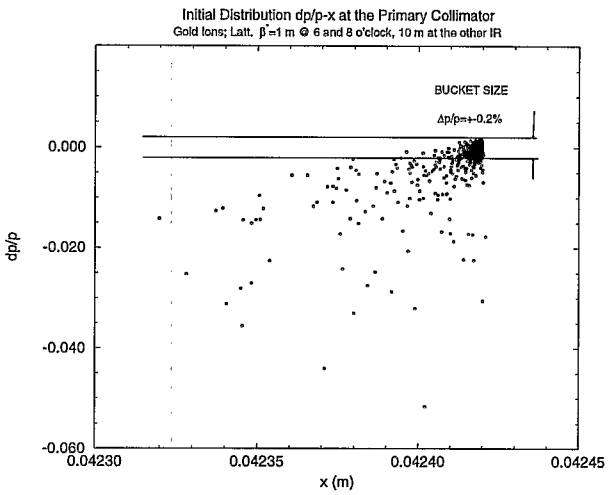

Figure 5: Initial momentum distribution of gold ions scattered from the primary collimator versus horizontal position.

in the horizontal phase space of the outscattered protons from the primary collimators is quite different with respect to already presented gold ion distributions. The major difference are significant number of the outscattered protons with opposite-positive angle of the primary collimator (see Fig. 6).

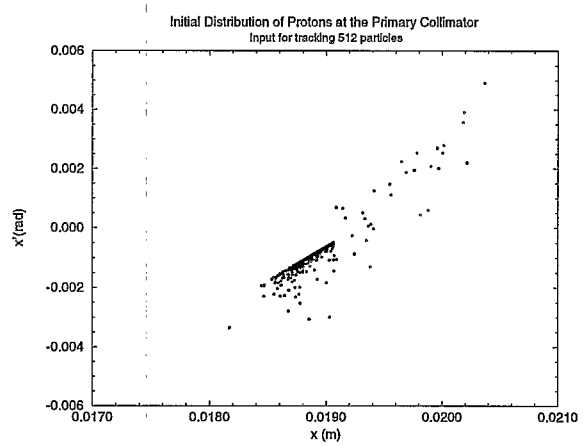

Figure 6: Initial distribution in x-x' phase space of protons outscattered from the primary collimator

Figures 6 and 7 present the initial proton distributions in x-x' and y-y' phase space, respectively.

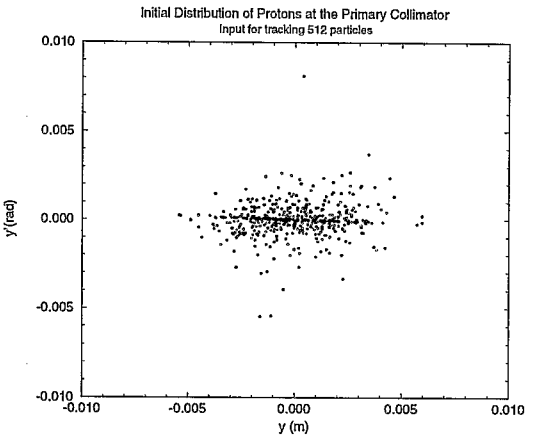

Figure 7: Initial distribution of protons in y-y' phase space outscattered from the primary collimator

4 PHASE SPACE DISTRIBUTION OF THE SCATTERED PARTICLES AROUND THE RINGS

The initial particle distribution is used as input for the tracking program TEAPOT [8]. The tracking was performed with the systematic and random multipoles within the quadrupoles and dipoles obtained from the measurement data, at the top energy of 100 GeV/nucleon for gold or 250 GeV for protons and for 256 turns. The misalignment and roll errors were obtained from the surveying data. The rms values for misalignment of the arc quadrupoles were Δx,y $\simeq$ 0.5 mm and $\Delta\theta$=0.5 mrad, while from the measurements of the triplet quadrupoles the roll and misalignment errors for the rms values were $\Delta\theta$=0.5 mrad and Δx,y=0.5 mm.

4.1 Longitudinal Phase Space

During tracking the RF voltage was included and the longitudinal motion of the surviving particles was monitored. Particles with momentum offsets within the bucket size limit executed synchrotron oscillations. Particles projections in the longitudinal phase space show in Fig. 8 that only particles within the bucket survive. Only few particles, which survived all 256 turns, finished almost one synchrotron oscillation. This is in accordance to the value used in tracking (synchrotron frequency used in the TEAPOT f=300 Hz) of $\simeq$260 turns for the full synchrotron oscillation. (It should be noted that the correct gold ion beam storage synchrotron frequency in RHIC is 326 Hz).

4.2 Transverse Phase Space Distribution

The transverse positions of the scattered particles on the first turn show that most of the particles with large momentum offsets are lost around the first bending elements. Particles outscattered from the primary collimator could

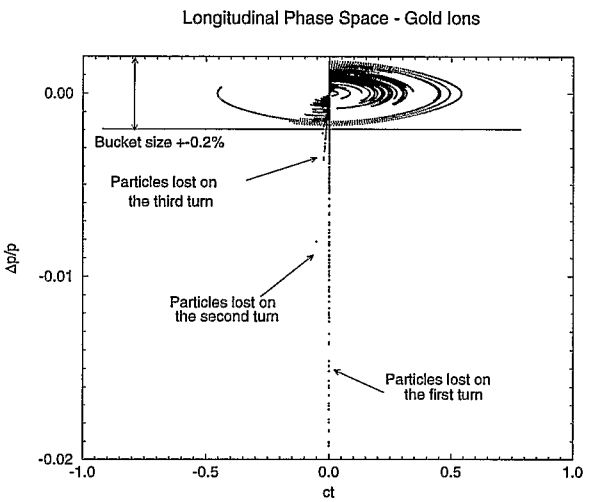

Figure 8: Longitudinal tracking

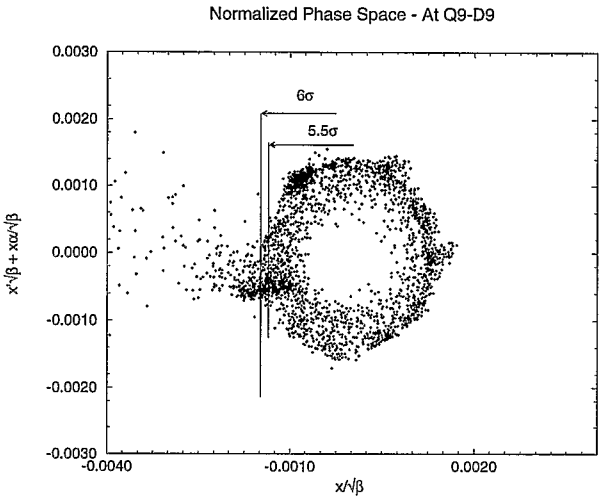

Figure 10: Optimum position of the secondary collimator

continue to make few or more turns around the accelerator. Their distributions in the horizontal phase space at a location $\simeq$30 m downstream of the primary collimator is presented in Fig. 9.

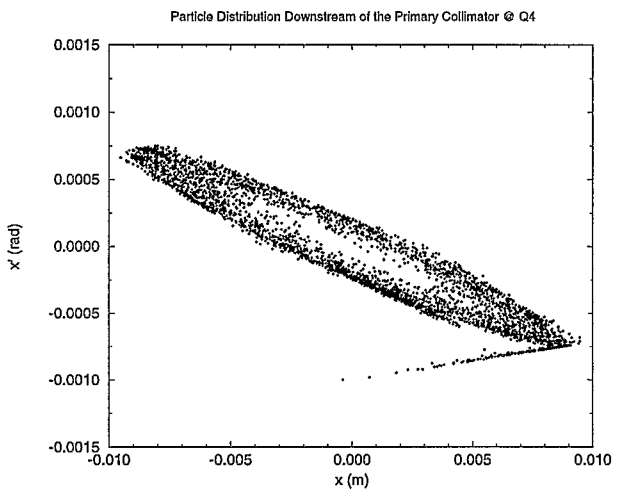

Figure 9: The outscattered particle's distribution in the x-x' phase space.

5 THE SECONDARY COLLIMATORS

Particles outscattered from the primary collimators could not only increase the beam halo due their large amplitudes but they can create secondary showers towards detectors due to their interaction with the walls of the limited apertures of the upstream triplet quadrupole magnets. The function of secondary collimators is to reduce the beam halo around experiments further. If the primary collimator jaws were set at 5.5 σ from the central axis it is preferable to have the secondary collimators retracted at 6.5 σ at least one σ further than the primary one. The secondary collimators in RHIC would have to fulfill their purpose for both outscattered particles heavy ions (gold ions) as well as the protons. As it is easy to see from Fig. 6 the large number of outscattered protons from the primary collimator have positive slope of the horizontal betatron function. To remove these particles, the preferable phase differences between the secondary betatron collimators and the primary ones, are [9] $\Delta\phi \simeq 15 - 30^o$ or $\Delta\phi \simeq 185 - 210^o$. The heavy ions, as it is presented for the gold ions in Figures 3 and 4, interact with the collimator's jaws differently. The preferable phase differences between the secondary and the primary betatron collimators which remove the largest amount of both outscattered protons and gold ions from the primary betatron collimators, are: $\Delta\phi \simeq 150 - 165^o$ or $\Delta\phi \simeq 330 - 345^o$. We determined the optimum positions for the secondary collimators by studying the outscattered particles' phase space distributions around the ring. We studied all three: x-x', y-y', and x-dp phase space distributions. As we already emphasized, the beam halo in the gold ion store is created by the IBS, when the high momenta particles escape the *rf* bucket. A previous study [10] has shown preferable positions in the RHIC lattice for the "momentum scrapers". We will show that our most preferable positions for the secondary betatron collimators coincide with the most desirable positions of the "momentum scrapers". Particle distribution in the horizontal betatron space is shown in the normalized phase space. The normalized phase space is defined by the Floquet' transformation [11] as:

$$\xi = \frac{x}{\sqrt{\beta}} \quad and \quad \chi = x'\sqrt{\beta} + \frac{x\alpha}{\sqrt{\beta}}, \qquad (3)$$

where the β and α are the Courant-Snyder functions, while x and x' are the offset and the slope of the horizontal position. The best positions (*Q9-D9 in the RHIC lattice*) for the secondary collimators are shown in Fig. 10. These positions (*Q9-D9 in the RHIC lattice*) were previously [10] selected due to the large value of the dispersion function ($D_x \simeq 1.5$ m @ Q9-D9 drift). The large amplitude of the particles at this position is a combination of two terms:

$$\sigma = \sqrt{\sigma_{twiss}^2 + \left(D_x \frac{dp}{p}\right)^2}. \quad (4)$$

The horizontal phase difference at the chosen location between the primary and the secondary collimator is 165^o.

5.1 *Particles' momenta at the secondary scraper*

Fig. 11 represents projections of the particles positions at the possible secondary collimator but in a different space. The horizontal axis represents particles' momenta, while the vertical axis is chosen for their horizontal positions.

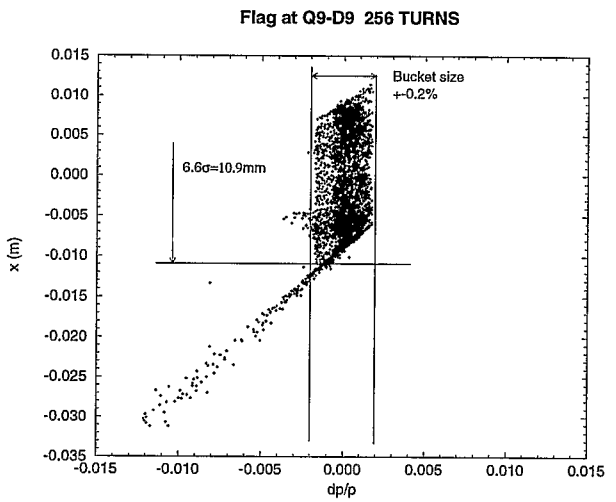

Figure 11: Horizontal positions of gold ions scattered from primary collimator at the secondary collimator with respect to their momenta.

This plot clearly shows the additional advantage of having the secondary scraper at this location. When the secondary scraper is set to a horizontal offset larger than 7σ, particles out of the bucket are eliminated. this location.

6 BEAM LOSS LOCATIONS IN THE RING

The RHIC lattice functions were transferred from the RHIC data base directly to the program TEAPOT. The aperture size of every element was present during the tracking. When a specific particle reaches the aperture limitation its tracking stops and the "loss" location, three coordinates, and an identification of particle are recorded. At the large detectors where the $\beta^* = 1$ m the strong focusing quadrupoles (as shown in Fig. 12) have their effective apertures reduced, due to the large values of the β functions. The losses of the outscattered particles from the primary collimator occur at these quadrupoles. The lost particles are presented on a logarithmic scale. Fig. 12 also shows losses at a set of magnets downstream of the primary collimator which are mostly due to the large momentum offset particles. The largest number of lost particles is at the strong focusing quadrupoles.

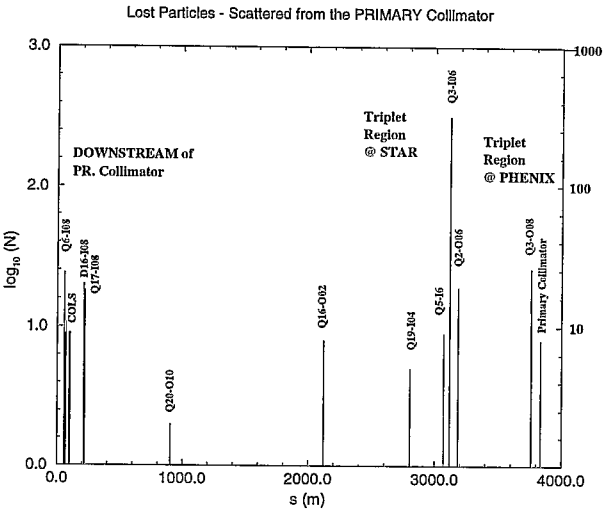

Figure 12: Losses around the ring from the primary collimator. The sample tracked consisted of 512 outscattered ions.

6.1 *Secondary Collimator Retraction Scan*

The efficiency of the secondary collimators was studied with the fixed position of the primary collimators at 5.5 σ. The tracking was performed as a function of the secondary

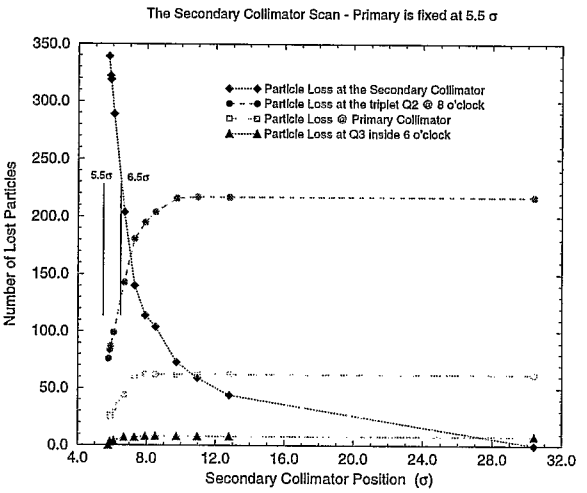

Figure 13: Distribution of losses during the secondary collimator scan.

collimator position. Fig. 13 shows number of lost parti-

cles at four selected locations with respect to the position of the secondary collimator obtained by tracking. Almost all outscattered particles from the primary collimator are lost during the 256 turns. When the secondary collimator jaws are fully retracted a large number of the outscatters will be lost again at the primary collimator. Particles which reached again the primary collimator were not transported through the collimator material by the *ELSHIM* code; they are assumed to be lost. When a retraction of the secondary collimator reached 11 σ the number of lost particles at both collimators became equal. A number of the lost particles at Q2 triplet quadrupole was dramatically lowered when the jaws of the secondary collimator reached 6.5 σ. The presented secondary collimator scan was obtained from the study of the *blue* ring, while the losses presented in Fig. 12 are obtained in the *yellow* ring.

7 CONCLUSIONS

The primary collimators in RHIC are important for many reasons:

- To remove the beam halo and reduce the background noise for the detectors.
- As a very good tool for beam diagnostics [9]: acceptance measurements, transverse particle distribution of the beam, frequency analysis of the beam loss rate, etc.

A combination of the primary and secondary betatron collimators can be used to remove not only the scattered particles from the primary collimator but also to remove particles out of the buckets. The secondary betatron collimators are effective only if the betatron phase difference between the two scraping stages is correctly chosen. Efficient momentum collimation [10] had already been reported at the same location, as it is the optimum position of the secondary betatron collimator (found in this study). It would be possible to create *macro buckets* with the use of the RHIC 28 MHz cavities to trap the particles outside of the buckets and scrape them [10]. The secondary collimator position determined in this study removes particles with large momentum offsets scattered from the primary collimator. It should be noted that losses from the primary collimators will still be the same in the same intersection region between the primary and secondary collimators. The spray at the triplets with the high values of β functions exists although it is significantly reduced.

8 REFERENCES

[1] A. J. Stevens, P.A. Thompson, and D. Trbojevic, *"Simulation of Detector Background Due to Beam Halo in RHIC"*, Internal Report Brookhaven National Laboratory, AD/RHIC/RD-117, October 1997, p.13.

[2] D. Trbojevic, A. J. Stevens, M.A. Harrison, F. Dell, and S. Peggs, *"A Study of Betatron and Momentum Collimators in RHIC"*, PAC97, Vancouver, Canada, May 1997, to be published.

[3] Jie Wei ,*"Magnet Quality and Collider Performance Prediction"*, Internal Note: RHIC/AP/117 (1996).

[4] A.Van Ginneken, *"Elastic scattering in thick targets and edge scattering"*, Physical Review D, Vol. 37, number 11, 1 June 1988, pp.3292-3307.

[5] A.Van Gineken, *"ELSHIM, Program to simulate Elastic Processes of Heavy Ions"*, BNL-47618, AD/RHIC-100, Informal Report, May 1992.

[6] L. Burnod and J.B. Jeanneret, *"Transverse Drift Speed Measurements of the Halo in a Hadron Collider"*, Proceedings of the Workshop on Advanced Beam Instrumentation, KEK, p. 375 (1988).

[7] W. Fischer, M. Giovannozzi and F. Schmidt, *"Dynamic aperture experiment at a synchrotron"*, Phys. Rev. E, Vol. 55, Number 3, p. 3507 (1997).

[8] L.Schachinger and R. Talman, *"A Thin Element Accelerator Program for Optics and Tracking"*, SSC Central Design Group, Internal Report SSC-52 (1985).

[9] M. Seidel, *"The Proton Collimation System of HERA"*, Dissertation, DESY 94-103, June 1994, Hamburg 1994.

[10] S. Peggs and G.F. Dell, *"Momentum Collimation at Q9"*, Report-no:RHIC/AP/78, November 1995.

[11] E.D. Courant and H.S. Snyder, *"Theory of the Alternating Gradient Synchrotron"*, Ann. Phys. **3**, 1 (1958).